

Supplementary Information for
**Vapor-Liquid-Solid Growth of Serrated GaN
Nanowires: Shape Selection via Kinetic
Frustration**

Characterization of as-grown nanowire sample

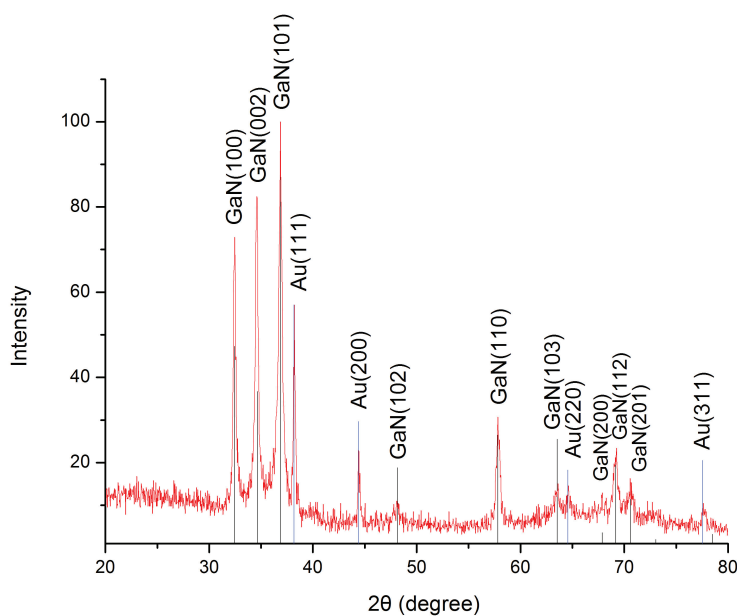


Figure 1: X-ray diffraction scan of an as-grown sample consisting of serrated and straight GaN nanowires indexed to the wurtzite phase with the experimental lattice parameters of $a = 3.194 \text{ \AA}$ and $c = 5.196 \text{ \AA}$. The a and c values indicate stress-free GaN crystal lattice [23]. The gold peaks are due to the capping catalyst particle.

Characterization of straight nanowires

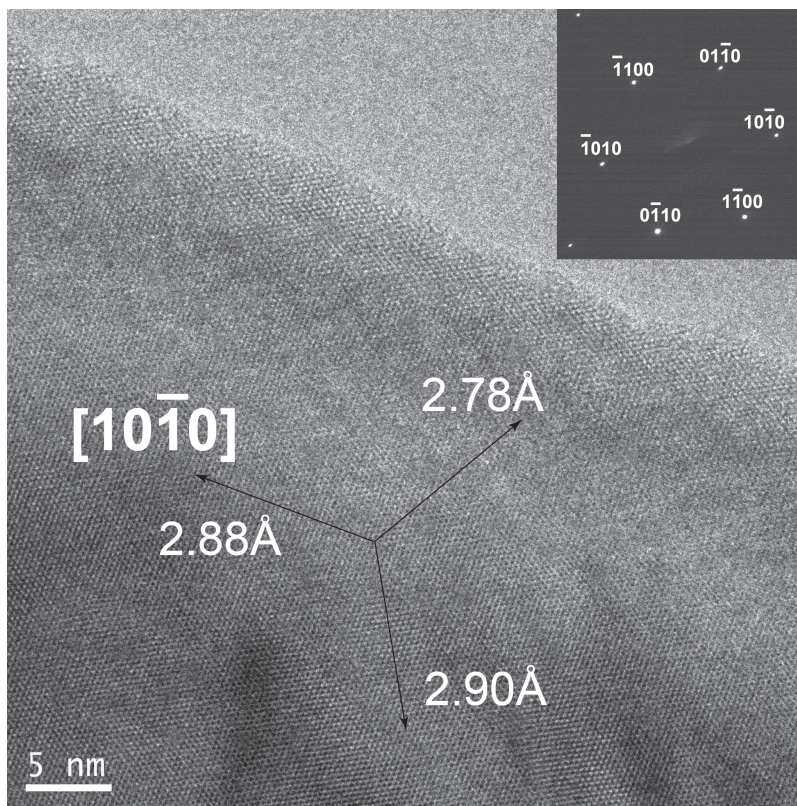


Figure 2: HRTEM image of a straight GaN nanowire viewed normal to the basal (0001) plane. The fringe spacing along the growth direction indicates non-polar growth along the $[10\bar{1}0]$ direction.

Characterization of serrated nanowires

Electron Backscatter Diffraction Analysis

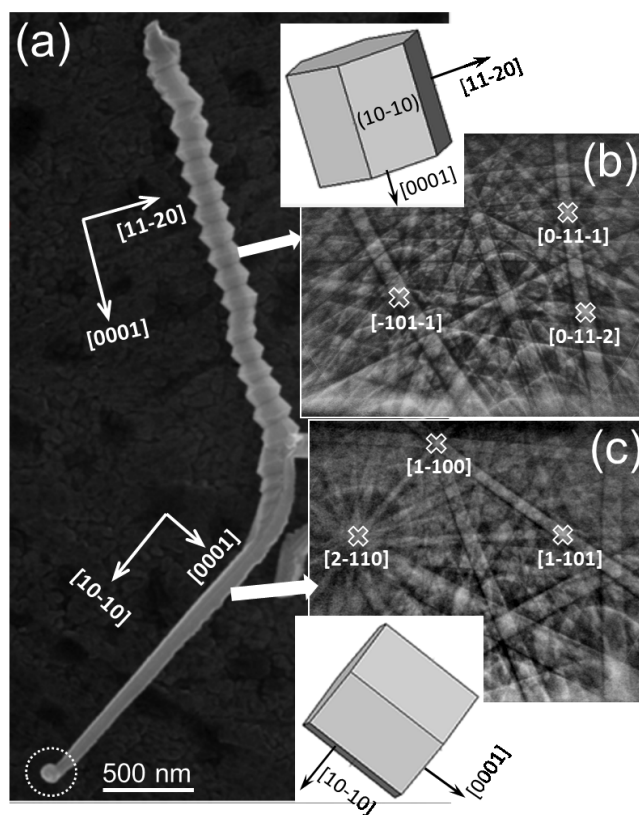


Figure 3: EBSD characterization of serrated nanowire that transitioned into straight nanowire. (a) SEM plan-view image of the whole nanowire capped by the Au catalyst particle (encircled with dashed line, bottom left). (b) EBSD pattern of the serrated segment with the simulated crystallographic orientation of the GaN unit cell (top left inset). Indexing of the EBSD pattern shows that the serrated nanowire grow along the [0001]-axis. (c) EBSD pattern of the straight nanowire segment with the simulated GaN unit cell (bottom left inset). The straight nanowire has a noticeably smaller size and the growth is along the non-polar $[10\bar{1}0]$ direction.

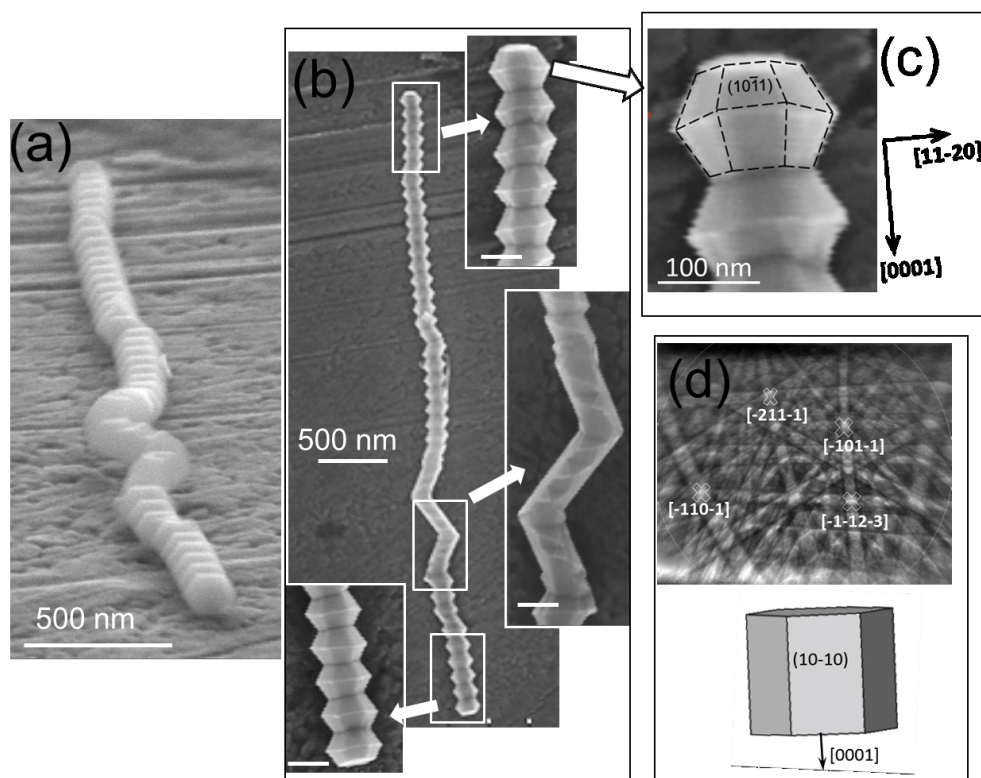


Figure 4: SEM (a)-(c) and EBSD (d) characterization of a serrated nanowire with small “zigzagged transition zone (shown in the middle inset in (b)) that reverts back to serrated growth (lower inset in (b)). SEM 70°-tilt image of the nanowire that was harvested from the as-grown sample; SEM plane-view image of the same nanowire with magnified top, middle and bottom segments in the insets (scale bar in each inset is 100 nm) EBSD characterization along the $[1010]$ direction identifies the growth along the polar axis enveloped by semi-polar $(10\bar{1}1)$ sidewall facets. (c) High-magnification SEM of the nanowire tip with labeled $\{10\bar{1}1\}$ sidewall facets and $[0001]$ growth axis as identified from the EBSD analysis (explained below in (d)); eye-guiding dashed lines indicate six out of twelve $\{10\bar{1}1\}$ facets in the truncated hexagonal bipyramid top segment. (d) Typical EBSD pattern from the nanowire with the simulated crystallographic orientation of the GaN unit cell. Conservation of the EBSD pattern collected from various points along the nanowire, including the serrated top, “zigzagged transition zone, and serrated bottom segments, indicates that the nanowire preserves the $[0001]$ growth axis and $(10\bar{1}0)$ in-plane surface orientation along its whole length. The $(10\bar{1}0)$ surface orientation unambiguously defines the side facets of truncated bipyramid segments to be $\{10\bar{1}1\}$ family (as labeled in (c)).

Supplementary Notes

Theoretical Model

We employ a near-equilibrium theoretical framework to relate the energetics of the nanowire-particle system to the V:III ratio at the growing nanowire front. The central aspect of Au-catalyzed GaN growth is the inherent bias in that N incorporation is limited to the contact line while Ga forms a liquid solution with Au diffuses through the particle. The relatively high growth temperature results in a liquid Au-Ga solution for sufficiently rich Ga in the gas phase. Then, the catalyst particle serves as a reservoir for Ga that changes its volume in accordance with the III:V ratio.

We begin with geometry-based scalings for the incorporation rates (atoms/time). The Ga incorporation rate scales with the exposed particle surface area,

$$\mathcal{I}^{Ga} = k_{lv}^{Ga} A_{lv} / \Omega_l^{Ga} \sim k_{lv}^{Ga} R^2 / \Omega_l^{Ga}, \quad (\text{S1})$$

where $k_{lv}^{Ga} \equiv k_{lv}^{Ga}(p_{Ga}, T)$ is the Ga catalysis rate at the droplet surface that depends on the reactor temperature and precursor gas partial pressure, A_d is the droplet surface area and Ω_l^{Ga} is the Ga atomic volume within the liquid particle. The nitrogen incorporation is assumed to occur along an annular ring of width δR around the contact line. The width is of the order of the truncating facet that is stabilized at the point where the polar [0001] facet meets the nanowire sidewalls. Then,

$$\mathcal{I}^N = k_c^N A_c / \Omega_s^N \sim k_c^N [R^2 - (R - \delta R)^2] / \Omega_s^N \approx k_c^N R \delta R / \Omega_s^N, \quad (\text{S2})$$

where $k_c^N \equiv k_c^N(p_{\text{NH}_3}, T)$ is the catalysis rate associated with NH_3 abstraction at the contact line and Ω_s^N is the nitrogen atomic volume.

The build-up of the excess Ga and N available for nucleation and growth at the particle-nanowire interface is controlled by their respective chemical potentials. Since Ga diffuses through the liquid particle, its excess is proportional to the difference in chemical potential between the liquid particle and the solid nanowire. In the limit of small supersaturations, the chemical potentials can be simplified as

$$\mu_s^{Ga} - \mu_{s(eq)}^{Ga} \sim \Omega_s^{Ga} \left[\sum_i \kappa_i^\gamma + \gamma_{lv} \kappa \right] \quad (\text{S3})$$

$$\mu_l^{Ga} - \mu_{l(eq)}^{Ga} \sim \ddot{G}(X_{l(eq)}^{Ga}) \left[X_l^{Ga} - X_{l(eq)}^{Ga} \right] + \Omega_l^{Ga} \gamma_{lv} \kappa. \quad (\text{S4})$$

Here, the reference potentials correspond to those for the ternary equilibrium between a solid GaN and a binary (Au-Ga) alloy at the growth temperature conveniently expressed in terms of the composition of the droplet, i.e. $\mu_{s(eq)}^{Ga} = \mu_{l(eq)}^{Ga}$. The change in the solid potential is the Laplace pressure exerted by the abutting liquid particle and the contributions of the

truncating and main facets. They are compactly expressed as the weighted mean curvatures $\kappa_i^\gamma = \pm \Lambda_i / L_i$ where Λ_i is the length (area) assigned to the facet on the Wulff plot and L_i is the actual facet length (area). The sign denotes the convexity of the each facet. The expression changes at the contact line as there is an additional term due to the capillary force exerted by the liquid surface tension and the solid-vapor interface energy, $\gamma_d \cos \theta_d - \gamma_{sv} \cos \alpha$, as shown in Fig. 4c. The liquid chemical potential increases linearly with the supersaturation $X_l^{Ga} - X_{l(eq)}^{Ga}$, where $X_{l(eq)}^{Ga}$ is the liquidus composition and $\ddot{G}(X_{l(eq)}^{Ga})$ is the second derivative of the free energy with respect to composition at equilibrium. The last term is the classical Gibbs-Thomson term due to the Laplace pressure within the liquid. Then, the change in Ga chemical potential due to abstraction from the vapor is

$$\Delta\mu^{Ga} \sim \ddot{G}\left(X_{l(eq)}^{Ga}\right) \left[X_l^{Ga} - X_{l(eq)}^{Ga}\right] + \Delta\Omega^{Ga} \gamma_d / R + \Omega_s^{Ga} \sum_i \kappa_i^\gamma \quad (\text{S5})$$

The nitrogen chemical potential of interest along contact line is set by the concentration (coverage) over the area of the surrounding annular ring that scales as $R\delta R$,

$$\Delta\mu^N \sim \ddot{G}\left(X_{c(eq)}^N\right) \left(X_c^N - X_{c(eq)}^N\right) + \gamma_d \sin \theta_d - \gamma_{sv} \cos \alpha \quad (\text{S6})$$

where $X_{c(eq)}^N$ is the equilibrium nitrogen coverage at the contact line and the last term is that due to the capillary force exerted by the liquid surface tension.

The concentration X_l^{Ga} and X^N evolve in accordance with the balance between the incoming and outgoing atomic flux (catalysis and nanowire growth, respectively). For an initially equilibrated particle-nanowire system, the steady-state values (increase per unit time) scale as

$$\frac{d\left(X_l^{Ga} - X_{l(eq)}^{Ga}\right)}{dt} = v \frac{d\left(\Delta X_l^{Ga}\right)}{dz} \sim \left(\mathcal{I}^N - \frac{vR^2}{\Omega}\right) \frac{\Omega_l^{Au}}{R^3} = \frac{\Omega_l^{Au}}{R} \left(\frac{k_{vl}^{Ga}}{\Omega_l^{Ga}} - \frac{v}{\Omega}\right) \quad (\text{S7})$$

$$\frac{d\left(X_c^N - X_{c(eq)}^N\right)}{dt} = v \frac{d\left(\Delta X^N\right)}{dz} \sim \left(k_c^N - v \frac{\Omega_s^N}{\Omega} \frac{R}{\delta R}\right), \quad (\text{S8})$$

where we have approximated the concentrations as the atom ratios of the relevant atomic species, i.e. $X_l^{Ga} \approx n^{Ga} / n^{Au}$ and $X^N \approx n^N / n_a^N$ where n_a^N is the available sites along the contact line that can be occupied by nitrogen. This is reasonable due to the low solubility of Ga (~ 5 at%) and slow N catalysis under the reactor conditions. Combining Eqs. S3-S4 and S7-S8, we arrive at scaling relations for the temporal increase in the chemical potentials within an initially equilibrated particle-nanowire upon exposure to the reactor conditions,

$$\frac{d\left(\Delta\mu^{Ga}\right)}{dt} \sim \ddot{G}\left(X_{l(eq)}^{Ga}\right) \Omega_l^{Au} \left(\frac{k_{vl}}{\Omega_l^{Ga}} - \frac{v}{\Omega}\right) - \frac{\Delta\Omega^{Ga} \gamma_d}{R^2} \frac{dR}{dz} + \frac{d\sum_i \kappa_i^\gamma}{dt} \quad (\text{S9})$$

$$\frac{d\left(\Delta\mu^N\right)}{dt} \sim \ddot{G}\left(X_{c(eq)}^N\right) \left(k_{ss}^N - v \frac{\Omega_s^N}{\Omega} \frac{R}{\delta R}\right) + \gamma_d \cos \theta_d \frac{d\theta_d}{dt}. \quad (\text{S10})$$

Equations S7-S10 capture the effect of geometry and processing conditions on the temporal increase in the concentrations and their effect on the chemical potentials of the two species. At microscopic time-scales, the growth is obviously not uniform; a critical supersaturation is required at the growth front for formation of a stable nucleus (interface-controlled regime). In the limit the catalysis is extremely slow, super-critical nucleus must wait for incorporation, and to a minor extent the diffusion, of Ga and/or N at the growth front catalysis-controlled regime which we analyze below.

Catalysis-limited growth

We consider the extreme case when the N incorporation is the rate-limiting event, i.e. the rate at which N becomes available through catalysis equals the rate at which it is absorbed into the growing nucleus, In essence, the growth velocity is kinetically limited by N-supply such that the N excess chemical potential is exactly at equilibrium and therefore constant, i.e. $d(\Delta\mu_c^N)/dt \approx 0$. Then, Eq. S8 yields the steady-state growth velocity,

$$v = \frac{\bar{\Omega}}{\Omega_s^N} \frac{\delta R}{R} k_c^N \quad (\text{S11})$$

Substituting in Eqs. S7-S8, we arrive at the temporal evolution of the concentration and chemical potential of Ga,

$$\frac{d(\Delta X^{Ga})}{dt} \sim \frac{\Omega_l^{Au}}{R} \left(\frac{k_{vl}^{Ga}}{\Omega_l^{Ga}} - \frac{\delta R}{R} \frac{k_c^N}{\Omega_s^N} \right) \quad (\text{S12})$$

$$\frac{d(\Delta\mu^{Ga})}{dt} \sim \frac{\ddot{G}(X_{l(eq)}^{Ga})\Omega_l^{Au}}{R} \left(\frac{k_{vl}^{Ga}}{\Omega_l^{Ga}} - \frac{\delta R}{R} \frac{k_c^N}{\Omega_s^N} \right) \quad (\text{S13})$$

Ignoring the differences in the atomic volume, we recover the relations in the main text (Eqs. 1 and 2) that we reproduce for completeness,

$$v \sim \frac{\delta R}{R} k_c^N \quad (\text{S14})$$

$$\frac{d(\Delta X^{Ga})}{dt} \sim \frac{1}{R} \left(k_{vl}^{Ga} - \frac{\delta R}{R} k_c^N \right), \quad \frac{d(\Delta X^N)}{dt} \sim 0 \quad (\text{S15})$$

$$\frac{d(\Delta\mu^{Ga})}{dt} \sim \frac{\ddot{G}(X_{l(eq)}^{Ga})}{R} \left(k_{vl} - \frac{\delta R}{R} k_c^N \right) + \frac{d\sum_i \kappa_i^\gamma}{dt}, \quad \frac{d\Delta\mu^N}{dt} \sim \gamma_d \cos \theta_d \frac{d\theta_d}{dt}. \quad (\text{S16})$$